Since January 2020 Elsevier has created a COVID-19 resource centre with free information in English and Mandarin on the novel coronavirus COVID-19. The COVID-19 resource centre is hosted on Elsevier Connect, the company's public news and information website.

Inorganic Chemistry Communications 134 (2021) 109029

Contents lists available at ScienceDirect

Inorganic Chemistry Communications

journal homepage: www.elsevier.com/locate/inoche

Synthesis, cytotoxicity and docking studies (with SARS-CoV-2) of water-soluble binuclear Ru-*p*-cymene complex holding indole thiosemicarbazone ligand

Jebiti Haribabu [a,b], Nithya Balakrishnan [a], Srividya Swaminathan [a], Jerome Peter [a,c], Dasararaju Gayathri [d], Cesar Echeverria [b], Nattamai Bhuvanesh [e], Ramasamy Karvembu [a,*]

[a] Department of Chemistry, National Institute of Technology, Tiruchirappalli 620015, India
[b] Facultad de Medicina, Universidad de Atacama, Copayapu 485, 1531772 Copiapo, Chile
[c] Division of Materials Science and Chemical Engineering (MSE), Hanyang University (ERICA), Ansan, Republic of Korea - 15588
[d] Centre of Advanced Study in Crystallography and Biophysics, University of Madras, Guindy Campus, Chennai 600025, India
[e] Department of Chemistry, Texas A & M University, College Station, TX 77842, USA

ARTICLE INFO

Keywords:
Thiosemicarbazone
Ru(II)-arene complex
Piano-stool
Cytotoxicity
SARS-CoV-2
Molecular docking

ABSTRACT

A water-soluble binuclear organometallic Ru-*p*-cymene complex [Ru(η^6-*p*-cymene)(η^2-L)]$_2$ (**1**) was prepared from (*E*)-2-((1H-indol-3-yl)methylene)-*N*-phenylhydrazine-1-carbothioamide (HL) and [RuCl$_2$(*p*-cymene)]$_2$ in methanol at room temperature under inert atmosphere. The structure of binuclear complex was analyzed by UV–Visible, FT-IR, NMR and mass spectroscopic methods. The solid-state structure of the complex was ascertained by single crystal X-ray diffraction technique. The complex exhibited *pseudo*-octahedral (piano-stool) geometry around Ru(II) ion. The cytotoxic property of the ligand and complex along with cisplatin was investigated against A549-lung, MCF-7-breast, HeLa-cervical, HepG-2-liver, T24-urinary bladder and EA.hy926-endothelial cancer cells, and Vero-kidney epithelial normal cells. The complex exhibited superior activity than cisplatin against A549, HeLa and T24 cancer cells with the IC$_{50}$ values of 7.70, 11.2, and 5.05 μM, respectively. The complexes were cytotoxic specifically to the cancer cells. Molecular docking studies showed good binding potential of the ligand and complex with the spike protein and main protease of SARS-CoV-2, indicating the promising role of these compounds as antiviral compounds.

1. Introduction

Cancer is one of the major health concerns in the present society, which affects nearly all the parts of the body. The most frequent cancer affecting the people worldwide is lung cancer which has claimed 1.76 million lives among 2.09 million cases in 2018. Similarly, in midst of women, breast cancer is the most common cancer affecting an average of 2.1 million women each year. It was recently estimated that 15% of the cancer-related deaths among women was due to breast cancer [1]. Early diagnosis approaches emphasize on administering the effective and timely treatment to the affected population [2]. Most of the cancer patients have a combination of treatments, such as surgery with chemotherapy and/or radiation therapy [3]. The idea of synthesizing transition metal complexes having chemotherapeutic properties has propagated due to an unmet clinical need for effective anticancer drugs [4].

Cisplatin, a Pt-based drug gained a widespread appreciation for its cytotoxic property, establishing the trend of using metal-based drugs in chemotherapy. Along with cisplatin, oxaliplatin, carboplatin, nedaplatin and lobaplatin are various other Pt(II) coordination compounds which are employed in the chemotherapy. However, acquired Pt resistance and the lack of cellular selectivity of these drugs have paved the way for the development of new alternatives based on other metals and their corresponding complexes [5]. Ruthenium(II/III) complexes have gained considerable interest as they have comparable ligand exchange kinetics to that of Pt. The *in vivo* mechanism of action of Ru complexes as anticancer agents is different from the conventional DNA-binding mechanism exhibited by cisplatin [6].

Some of the Ru(III) complexes namely indazolium *trans*-tetrachloro*bis*(1H-indazole)ruthenate(III) (KP1019) and sodium *trans*-

* Corresponding author.
E-mail address: kar@nitt.edu (R. Karvembu).

https://doi.org/10.1016/j.inoche.2021.109029
Received 6 September 2021; Received in revised form 21 October 2021; Accepted 25 October 2021
Available online 28 October 2021

tetrachloro*bis*(1H-indazole)ruthenate(III) (NKP-1339) have already entered the clinical trials and have shown promise in chemical model systems both *in vitro* and *in vivo* [7–8]. The first anticancer Ru-arene system *viz*., [Ru(η^6-benzene)(metronidazole)Cl_2] was reported in 1992 by Tocher *et al* [9]. In 2001, Dyson *et al*., [10] assessed the anticancer properties of complexes of the type [(η^6-*p*-cymene)Ru(pta)Cl_2] (RAPTA-C). Similarly in the same year, Sadler and co-workers had reported the mechanism of action of their synthesized complexes of the type [Ru(η^6-arene)(en)(Cl)]$^+$ (RM175) [11]. So, the anticancer potential of the half-sandwich Ru(II)-arene complexes of general formula [Ru(η^6-arene)(X)(YZ)], wherein X is a leaving ligand and YZ is a bidendate chelating ligand, is currently of great interest [12–15].

Indoles are thought as privileged moieties in biological systems due to the valuable potentials they possess in human health care. This class of compounds is constituted in proteins in the form of tryptophan and in bioactive alkaloid compounds like strychnine and lysergic acid diethylamide (LSD), marine natural products and fungal metabolites. In addition, the backbone structures of many drugs like vincristine and vinblastine (anticancer), sumatriptan (antimigraine), indomethacin [non-steroidal anti-inflammatory drug (NSAID)] and pindolol (antihypertensive) are composed of indole fragment as incorporation of such a versatile pharmacophore enhances their therapeutic potential [16,17].

Thiosemicarbazones (TSCs) are mainly bidentate chelating ligands possessing a wide range of pharmacological properties such as antifungal, antibacterial, antioxidant, antitumor, *etc*. TSCs form stable metal complexes mainly *via* azomethine nitrogen and thionic sulphur, which in turn have better biological activities than their parent ligands [18–20]. TSCs-anchored half-sandwich Ru(II)-arene complexes are thought as promising therapeutic agents [21–23]. Usually, in Ru(II)-arene complexes bearing TSCs, thiocarbonyl sulphur coordinates with the metal ion either in the thione or thiol form, forming a five-membered chelate ring, resulting in mononuclear cationic or neutral complexes. Although there are many reports on Ru(II)-arene complexes with TSCs, very few reports deal with binuclear Ru(II)-arene complexes where TSC ligands form either five- or four-membered chelate ring *via* bidentate (N^1,S/N^2,S) chelation to Ru(II) ion. Su *et al*., had synthesized the binuclear Ru-arene complexes in a two-step reaction [24]. Our group is actively involved in the study of DNA/BSA binding and anticancer activity of the Ru-arene complexes with thiosemicarbazone/thiourea ligands [25–28]. The reported complexes show good activity against cancer cells, inducing cell death through apoptosis. We previously reported the synthesis and DFT modelling of water soluble mono- and binuclear Ru(II)-*p*-cymene complexes formed based on the *N*-terminal substitution of indole TSC ligands, and the complexes exhibited potential anticancer activity against various cancer cells through apoptosis cell death [21]. In the present study, the synthesis of water-soluble binuclear Ru(II)-*p*-cymene complex was achieved by using *N*-phenyl indole TSC ligand.

Transition metal complexes have advantages over other small molecular drugs by virtue of wide spectrum of oxidation number, coordination states, multi-target effect, *etc*. Metal complexes may produce favorable multi-target effects on the pathogens and viruses due to their unique metal centers [29]. Very rapid spread of SARS-CoV-2 has substantially increased the research towards the development of potential COVID-19 antiviral drugs and vaccines. Solubility is an important factor for the drug to enter the systemic circulation for showing a pharmacological response. Drugs that lack aqueous solubility show poor bioavailability and decreased absorption, which directly affect the therapeutic potency of the drugs. Hence, the need for water soluble drugs is at large. These factors motivated us to design and synthesize a water-soluble binuclear Ru(II)-*p*-cymene complex in a one-step reaction. This complex was characterized by analytical and various spectroscopic tools. The piano-stool structure of the complex was determined by single crystal X-ray diffraction study. The anticancer activity of the compounds was investigated against six cancer and one normal cell lines. Molecular docking studies of the compounds with the spike protein and main protease of SARS-CoV-2 were investigated.

2. Experimental section

2.1. Materials and methods

All the required chemicals were purchased from Sigma Aldrich/Merck. The melting points were determined on a Lab India instrument and are uncorrected. FT-IR spectra were obtained as KBr pellets using a Nicolet-iS5 spectrophotometer. UV–Visible spectra were recorded using a Shimadzu-2600 spectrophotometer. ^{1}H NMR spectra were recorded in $CDCl_3$ by using TMS as an internal standard on a Bruker 400 MHz spectrometer.

2.2. Synthesis of the binuclear Ru-p-cymene complex

(*E*)-2-((1H-indol-3-yl)methylene)-N-phenylhydrazine-1-carbothioamide (HL) was reported in our earlier publications [17,18,30]. This indole based TSC ligand (HL, 58.8 mg, 0.02 mmol, 2 equiv.) in methanol (3 mL) was added to the suspension of [$RuCl_2$(η^6-*p*-cymene)]$_2$ precursor (61.2 mg, 0.01 mmol, 1 equiv.) in methanol (2 mL), and the resulting red solution was stirred at room temperature for 70 min. The solution was concentrated to 2–3 mL under reduced pressure, and addition of hexane (20 mL) gave an orange color solid. The product was collected by filtration, washed with hexane and dried in *vacuo*. The suitable yellow block crystals for X-ray diffraction (XRD) were grown by slow evaporation of the binuclear complex in dichloromethane with 2 drops of N,N-dimethylformamide (DMF).

[Ru(η^6-*p*-cymene)(η^2-L)]$_2$ (**1**): Yield: 79%. Color: Orange. M.p. 236 °C. Anal. Calc. $C_{52}H_{54}Cl_2N_8S_2Ru_2$ (%): C, 55.36; H, 4.82; N, 9.93; S, 5.68. Found: C, 55.41; H, 4.73; N, 10.05; S, 5.59. UV–Vis (DMSO): λ_{max}, nm 269, 337, 427. FT-IR (KBr): υ, cm^{-1} 3430, 3307 (N–H), 1494 (C=N), 1217 (C–S). ^{1}H NMR (500 MHz, $CDCl_3$/TMS): δ, ppm 14.49 (s, 2H, indole N–H), 10.60 (s, 2H, CH=N), 9.05 (s, 2H, indole CH), 8.80 (s, 2H, N*H*–C_6H_5), 7.55 (d, J = 7.0 Hz, 4H, aromatic), 7.50 (d, J = 7.2 Hz, 4H, aromatic), 7.32 (d, J = 7.6 Hz, 4H, aromatic), 7.21 (d, J = 7.2 Hz, 4H, aromatic), 7.18 (d, J = 7.2 Hz, 2H, aromatic), 5.50–5.00 (m, 8H, aromatic-H of *p*-cymene), 2.65–2.60 (m, 2H, C*H*(CH_3)$_2$ of *p*-cymene), 2.01 (s, 6H, CH_3 of *p*-cymene), 1.12 (d, J = 6.4 Hz, 6H, CH(C*H*$_3$) of *p*-cymene), 1.06 (d, J = 6.4 Hz, 6H, CH(C*H*$_3$) of *p*-cymene).

2.3. Single crystal X-ray diffraction

X-ray diffraction data for complex **1** was collected from a Bruker Quest X-ray (fixed-chi geometry) diffractometer. The X-ray radiation employed was produced from a Mo-Iμs X-ray tube (K_α = 0.71073 Å). APEX3 software [31–33] was used to control the goniometer as well as for gathering the integrated intensity information for each reflection. The obtained data were corrected from absorption effects using the absorption correction program SADABS. Rest of the calculations and confirmations were done using the program PLATON (ADDSYM) [34]. Finally the structures were plotted and the final data were refined using the software Olex2 [35].

2.4. Stability studies

The stability of complex was analyzed by monitoring the electronic spectra at a temperature of 27 °C over a period of 24 h in 1:99 DMSO-water (*v/v*) solution.

2.5. MTT assay

The *in vitro* cytotoxicity of ligand and its Ru(II) complex was evaluated using 3-(4,5-dimethylthiazol-2yl)-2,5-diphenyltetraazolium bromide (MTT) assay, against human lung (A549), human breast (MCF-7), human cervical (HeLa), human liver (HepG-2), human urinary bladder

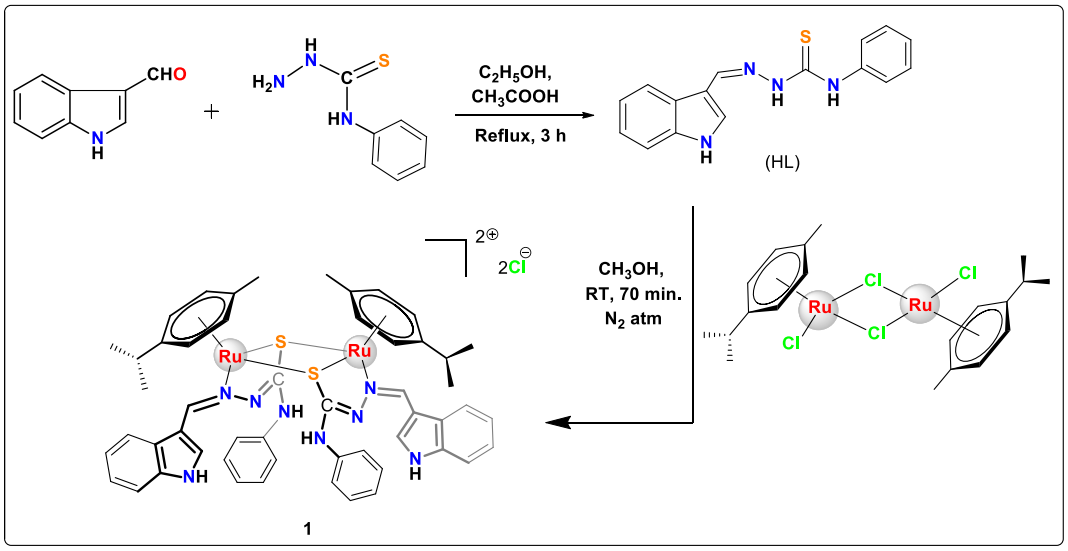

Scheme 1. Synthesis of the binuclear Ru-*p*-cymene complex with indole TSC ligand.

(T24) and human endothelial (EA.hy926) cancer cell lines, and kidney epithelial-from the African green monkey (Vero) normal cell line. Cells were seeded in 96-well plates at a concentration of 1×10^4 cells per well in Dulbecco's modified Eagle's medium (DMEM; A549, MCF-7, HeLa, HepG-2 and EA.hy926) / McCoy's 5a medium (T24) / Roswell Park Memorial Institute medium (RPMI-1640; Vero) and incubated for 24 h at 37 °C. Then compounds to be tested (in known concentration) were seeded into the wells after dissolving them in DMSO followed by the addition of 10 μL of MTT [5 mg/mL in phosphate-buffered saline (PBS)] dye to each well [36]. The cell plates were incubated at 37 °C until the intracellular purple formazan crystals formed due to the NADPH released by viable cells were visible under microscope. The excess MTT and media were removed and the solubilizing agent like DMSO (100 μL) was added and triturated. In order to lyse the cells and dissolve the purple crystals, the plates were again incubated at 37 °C for 2 h. Finally the absorbance was read in the multi-well ELISA reader at 570 nm. The assay was repeated in triplicate and the mean absorbance and standard deviation were calculated. IC_{50} values were determined as the concentration of corresponding compound that produced 50% reduction of cell viability [17].

2.6. Molecular docking

The structures of HL, complex **1**, chloroquine, hydroxychloroquine and remdesivir were converted into the pdb format using Chimera [37], which were then given as input to the AutoDock 4.2 [38]. After adding the Gasteiger charges, the polar hydrogens were merged and then the compounds were saved in pdbqt format which is a special file format used by the AutoDock, containing information about the partial charges (Q), atom type (T) and rotatable bonds of the compounds.

The receptors' crystallographic structures were retrieved from the protein data bank (PDB) [39–40]. SARS-CoV-2 spike protein (PDB id: 6M0J) [41] and the main protease (PDB id: 6Y2F) [42] structures in their pdb formats were given as input to the AutoDock, and further receptor preparations were carried out in AutoDock tools. For the spike protein, the ACE2 receptor was removed from the complex for carrying out molecular docking. The heteroatoms and water molecules were removed from both the proteins, after which the polar hydrogens and Kollman charges were assigned. The prepared proteins were then saved in pdbqt format. Interaction maps or the affinity grid maps were generated for the active site of the receptors prior to the actual docking process using the Autogrid program. Lamarckian genetic algorithm (LGA) was used to find the best possible conformation of the compounds binding with the receptors. Here, the protein was kept rigid while the ligand was flexible in the active site to find its conformation with the minimum binding energy. AutoDock program was used for docking of the compounds with the receptors. The docked conformations were analyzed using AutoDock tools. The conformations were ranked according to their binding energy, and the one with the lowest binding energy was the stable conformation of compound. The compound interactions at the binding site were analyzed using Chimera.

3. Results and discussion

3.1. Synthesis of the complex

(*E*)-2-((1H-indol-3-yl)methylene)-*N*-phenylhydrazine-1-carbothioamide (HL) was prepared from indole-3-carboxaldehyde and 4-methyl thiosemicarbazide in the presence of acetic acid [17,18,30]. Binuclear Ru-*p*-cymene complex (**1**) was synthesized from HL and $[RuCl_2(p\text{-cymene})]_2$ in 2:1 M ratio in methanol as shown in Scheme 1. The binuclear complex was well ascertained by elemental analysis, and various spectroscopic and single crystal XRD tools. The complex was soluble in water and organic solvents such as dichloromethane, chloroform, methanol, ethanol, DMF, DMSO, *etc*.

3.2. Confirmation of formation of complex *1*

3.2.1. UV–Vis spectroscopy

The UV–Visible spectrum (Fig. S1) of complex has been recorded in DMSO. Complex **1** showed two bands at 269 and 337 nm, which corresponded to $\pi \rightarrow \pi^*$ and $n \rightarrow \pi^*$ (intraligand) transitions, respectively. The $d \rightarrow d$ transition in complex was characterized by a new band observed at 427 nm [21].

3.2.2. IR spectroscopy

In the IR spectrum of complex **1**, the C–N band was observed at 1494 cm^{-1} while the same band in the spectrum of ligand was found at 1549 cm^{-1}, indicating the coordination of azomethine N of TSC ligand to Ru (II) ion (Fig. S2). The sulphur atom of ligand coordinated as thiolate (C–S) to Ru(II) center as demonstrated by a band at 1217 cm^{-1} in the spectrum of complex **1** wherein a decrease in frequency was seen compared to that of the ligand (1287 cm^{-1}) [21–23].

3.2.3. NMR spectroscopy

In the ^1H NMR spectrum of complex **1**, indole N–H, azomethine C–H

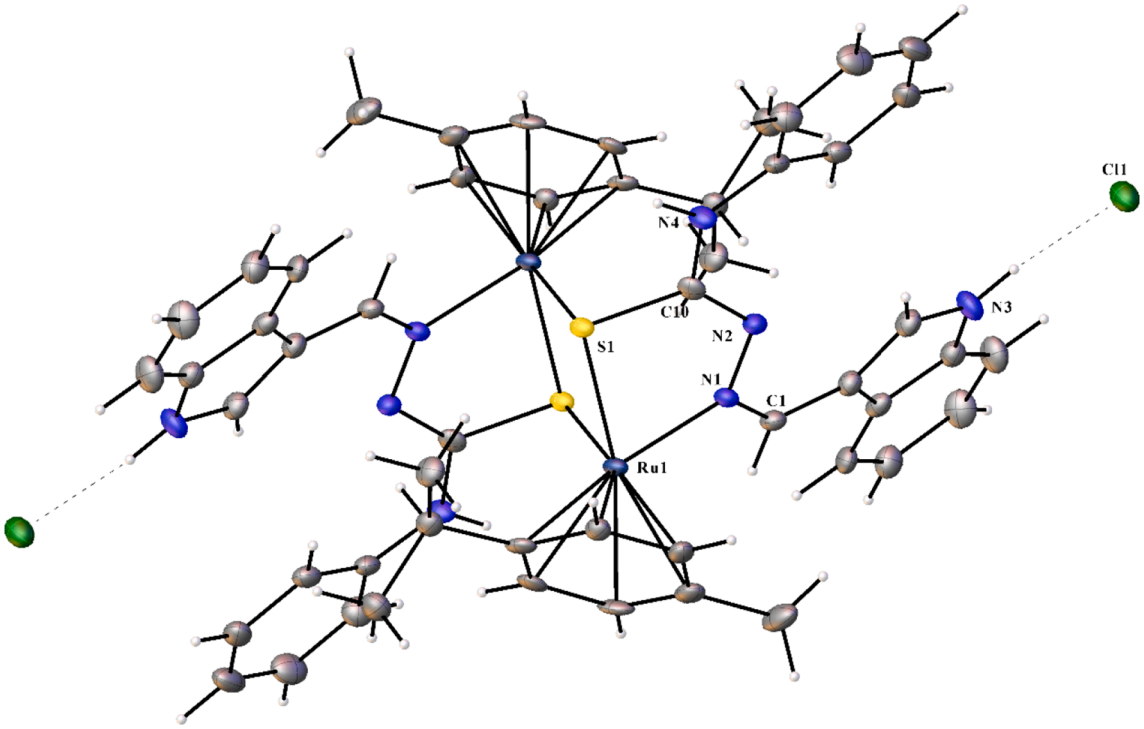

Fig. 1. Solid-state structure of **1** (50% probability level). Selected atoms are labelled for clarity. N–H···Cl^- hydrogen bonding interactions are shown in dashes.

and indole C–H protons gave signals at 14.49, 10.60 and 9.05 ppm, respectively, which were found to be deshielded due to coordination with electron deficient Ru(II) center as compared to the free ligand [12.17 (indole N–H), 8.33 (azomethine C–H) and 8.13 ppm (indole C–H)]. The isopropyl C–H and methyl protons in *p*-cymene were shielded and resonated at 2.65–2.60 and 1.06–1.12 ppm, respectively. The *p*-cymene methyl and aromatic protons were also shielded and gave signals at 2.01 and 5.00–5.50 ppm (Fig. S3), respectively [22].

3.2.4. Crystal structure

Complex **1** crystallized in monoclinic crystal system with space group $P2_1/n$ (Fig. 1). The crystal data and refinement parameters are provided in Table S1. The complex adopted a binuclear configuration with two Ru ions being connected by two bridged sulphur atoms of the TSC ligands forming a Ru_2S_2 core. The four-membered core with the bond lengths and angles of 2.422(10) [Ru(1)–S(1)#1] / 2.344(9) [Ru(1)–S(1)] Å and 80.68(4) S(1)–Ru(1)–S(1)#1 / 99.32(4)° [Ru(1)–S(1)–Ru(1)#1], respectively, was not regular or planar. Each [(η^6-*p*-cymene)Ru(*N*,*S*-TSC)]$^+$ moiety in the binuclear structure displayed the classical 'piano-stool' geometry wherein Ru(II) ion was coordinated by a spectator *p*-cymene ligand and the chelating (*N*,*S*) TSC ligand in *pseudo*-octahedral fashion. The distance between the Ru ion and the centroid of aromatic ring of *p*-cymene was 1.846(4) Å. The bond distances and angles around the Ru ion were as follows: Ru–N, 2.080(3) Å; N(1)–Ru(1)–S(1), 80.78(9)/78.71(9)°, which were comparable to those of the similar compounds (Table S2) [12,24,43]. The chloride counter ion involved in hydrogen bonding with the indole N–H and terminal NH with the distances of 2.278 and 2.354 Å, respectively. These types of hydrogen bonds are rare in Ru-arene complexes containing TSC ligands, and they may play a subtle role in medicinal and bioorganometallic chemistry.

3.3. Stability of the complex

The therapeutic potential of a metallodrug basically depends on its stability in the aqueous media. As the biological studies are normally done in 1% DMSO-water mixture, it is essential to know the stability of complex in this media for a period of 24 h. The UV–Visible spectral profile for complex **1** is shown in Fig. S4. The absorbance spectra of the complex recorded immediately and after 24 h did not display any noticeable change both in the intensities and positions of the bands, which clearly indicated the stability of complex under physiological conditions [15,25,44].

3.4. In vitro cytotoxicity

The cytotoxicity of the ligand, complex and cisplatin was assessed against a panel of human cancer cell lines such as lung cancer (A549), breast cancer (MCF-7), cervical cancer (HeLa), liver cancer (HepG-2), urinary bladder cancer (T24) and endothelial cancer (EA.hy926), and kidney epithelial normal (Vero) cells. The cytotoxic abilities after 24 h of incubation are expressed as IC_{50} values (Figs. 2 and 3, Table 1). The free ligand demonstrated cytotoxicity against A549 and MCF-7 cell lines with the IC_{50} values of > 50 μM, whereas its complex showed the cytotoxicity with the values of 7.70 and 28.3 μM, respectively. Similarly, the complex could show the effective cytotoxic profile against HeLa cells with an IC_{50} value of 11.2 μM (For the ligand, it is 46.2 μM). The complex showed significant cytotoxicity (22.8 and 5.05 μM) against HepG-2 and T24 cancer cells. This cytotoxicity was much higher than that observed for the ligand (>50 μM) and cisplatin (>50 μM). The superior cytotoxicity currently exhibited by the complex against T24 cancer cells is one of the phenomenal results found in the literature [45]. Also, the complex showed cytotoxicity of 18.5 μM against EA.hy926 cancer cells, whereas the positive control (cisplatin) exhibited lower cytotoxicity of 28.5 μM. The IC_{50} values of cisplatin for all other cell lines were found under similar conditions, which were reported by us earlier [15]. In a nutshell, the complex had a superior cytotoxic activity in all, over cisplatin except for MCF-7 cell line. Fortunately, both the ligand and complex exhibited higher IC_{50} values against normal monkey kidney (Vero) cells (100 μM), indicating the specificity of both against cancer cells. Even cisplatin exhibited a moderate cytotoxicity against the normal cells, unlike the synthesized compounds. The activity of complex was comparable to that of similar Ru-*p*-cymene complexes containing TSC ligands (Chart 1, Table 1) [21–24,46] and other ruthenium

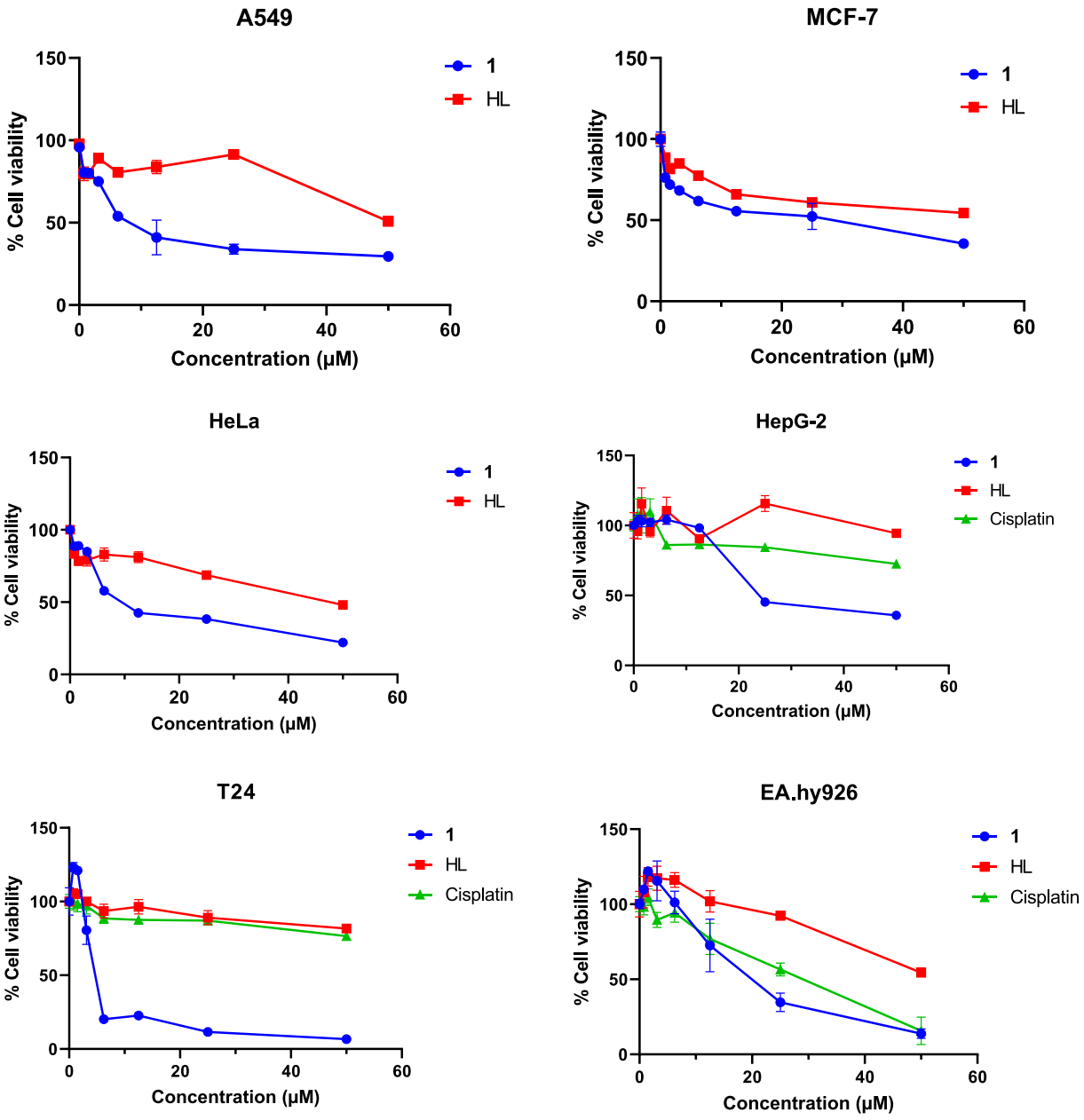

Fig. 2. Anticancer property of the compounds against A549, MCF-7, HeLa, HepG-2, T24 and EA.hy926 cancer cells. Results are mean ± SD.

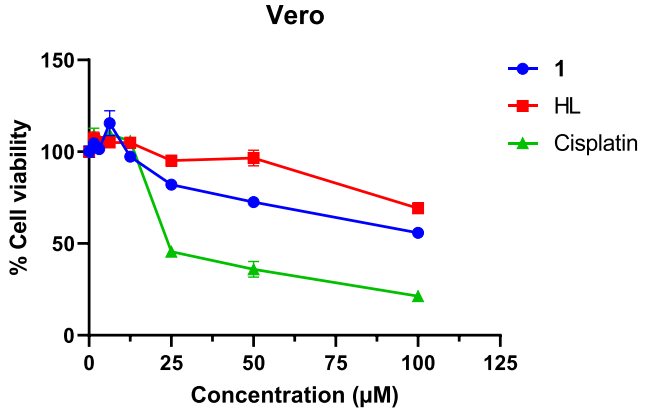

Fig. 3. Anticancer property of HL, **1** and cisplatin against Vero normal cells. Results are mean ± SD.

Table 1
IC_{50} values of HL, **1**, other reported Ru-*p*-cymene TSC complexes and cisplatin in A549, MCF-7, HeLa, HepG-2, T24 and EA.hy926 cancer and Vero normal cells as calculated by MTT assay.

Compound	IC_{50} (μM)						
	A549	MCF-7	HeLa	HepG-2	T24	EA.hy926	Vero
HL	>50	>50	46.2	>50	>50	>50	>100
1	7.70	28.3	11.2	22.8	5.05	18.5	>100
2[21]	–	18.05	–	–	–	–	–
3[46]	–	8.7	–	–	–	–	–
4[22]	35.3	–	–	11.5	–	–	–
5[22]	49.3	–	–	62.7	–	–	–
6[23]	–	5.18	–	–	–	–	–
7[24]		–	16.8	19.3	–	–	–
Cisplatin	18.0[15]	23.7[15]	22.4[15]	>50	>50	28.5	31.8

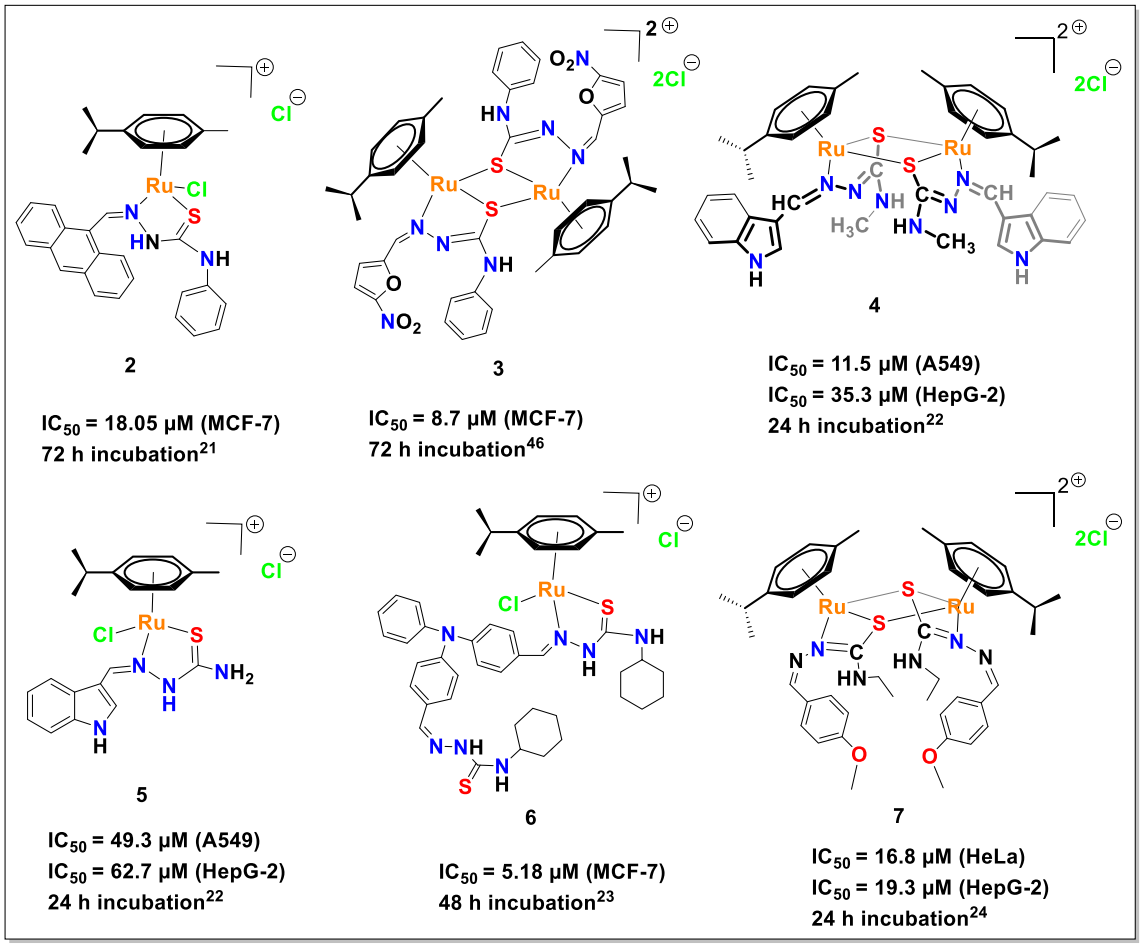

Chart 1. Anticancer activity of previously reported Ru-*p*-cymene complexes containing TSC ligand(s).

compounds [47–51].

3.5. Interaction with the spike protein and main protease of SARS-CoV-2

As Ru complexes and TSC derivatives are known to possess antiviral properties, we aimed to perform *in silico* molecular docking to understand the interaction of the compounds (HL and complex **1**) with the spike protein and main protease of SARS-CoV-2. Spike protein of SARS-CoV-2 binds to the host cell receptor and facilitates virus-cell membrane fusion, which is the primary key in the process of virus invasion into the host cell [41]. In the translation process, open reading frames ORF1a and ORF1b of SARS-CoV-2 genomic RNA produce two polyproteins, pp1a and pp1ab, which mediate all the functions required for the viral gene expression and replication. Several non-structural proteins are co-/post-translationally released from pp1a and pp1ab upon proteolytic cleavage by two cysteine proteases – papain-like protease and chymotrypsin-like protease (main protease). Main protease releases majority of non-structural proteins from the polyproteins and plays a pivotal role in the proteolytic activity of the viral replication process [42]. Both the spike protein and main protease are the key target enzymes in the drug discovery process against SARS-CoV-2.

To compare the binding energy and active site interactions of HL and complex **1** with the spike protein and main protease, we have performed molecular docking of antiviral drugs (chloroquine, hydroxychloroquine and remdesivir, Chart S1) with the target enzymes. For the spike protein, the grid was formed at the active site of the protein comprising of Tyr449, Tyr453, Asn487, Phe486, Tyr489, Gln493, Gly496, Gln498 Thr500, Gly502, Tyr505 amino acids with grid spacing and dimension of 0.500 Å and 36 × 78 × 36 Å, respectively [52]. For the main protease, a

Table 2
Binding energy and interactions of the compounds with SARS-CoV-2.

Compound	Binding energy (kcal/mol)		Active site residues involved in interactions	
	Spike protein	Main protease	Spike protein	Main protease
Chloroquine	−4.40	−6.47	R403, Y453, Q493, Y495, Q498, N501, Y505	C145, H163, E166, P168, H172, T190, Q192
Hydroxychloroquine	−4.19	−6.68	R403, Y453, Q493, Y495, F497, N501, Y505	F140, S144, C145, H163, M165, E166, H172, T190, Q192
Remdesivir	−3.78	−7.16	R403, E406, Y449, Y453, Q493, Y495, Q498, N501	H41, M49, F140, S144, C145, H163, M165, E166, L167, R188, Q189, Q192
HL	−6.46	−7.30	R403, E406, Y453, Q493, Y495, F497, N501, Y505	H41, M49, N142, S144, C145, H163, M165, E166, D187, Q192
1	−7.46	−9.39	R403, Y449, Y453, Q493, S494, Y495, F497, N501, Y505	T25, H41, C44, Y54, M49, C145, H164, D187, R188, Q192

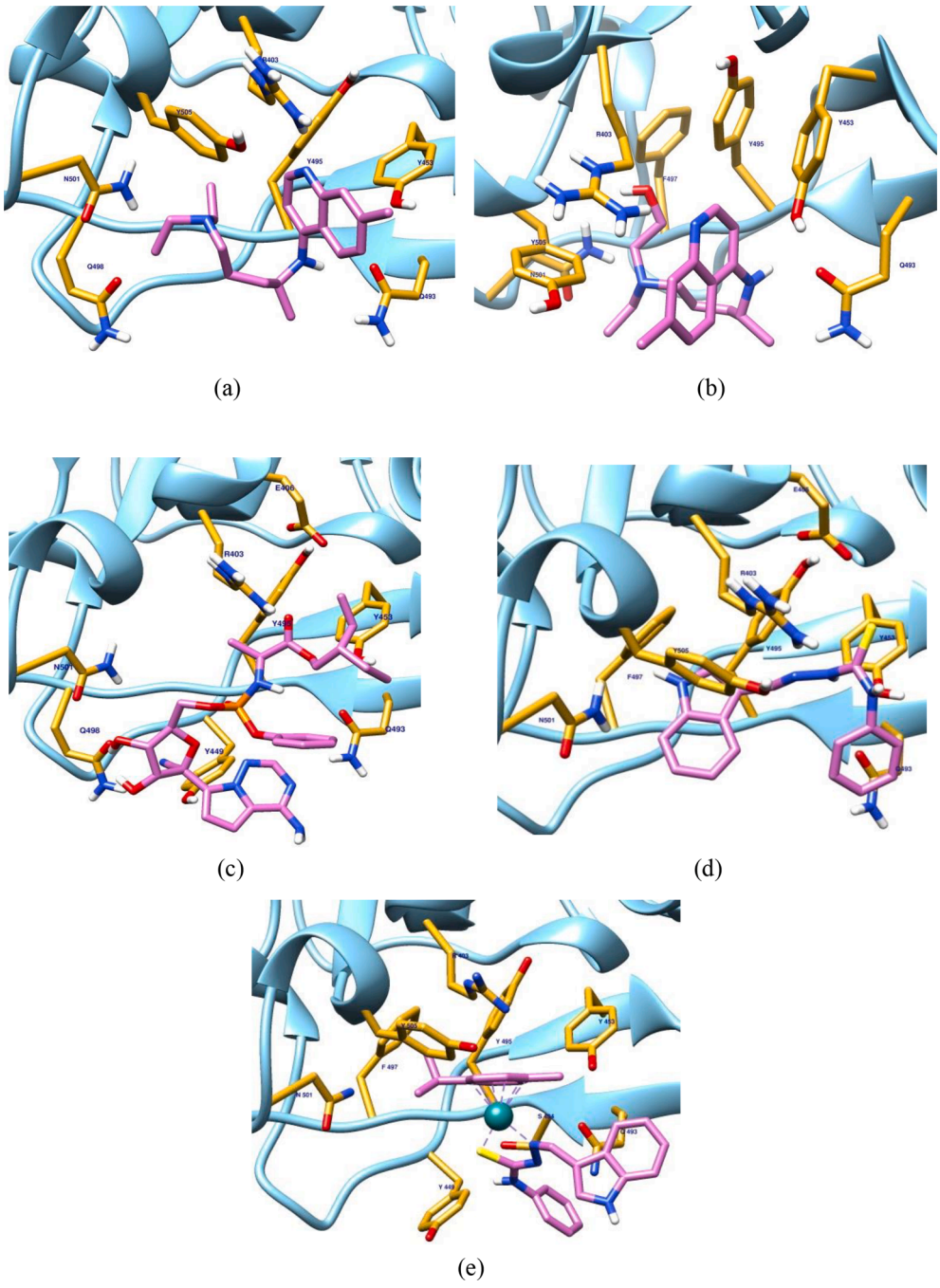

Fig. 4. Docked conformation of (a) chloroquine (b) hydroxychloroqine (c) remdesivir (d) HL and (e) complex **1** at the active site of SARS-CoV-2 spike protein.

grid box of dimensions 54 × 68 × 70 Å and 0.375 Å spacing was generated based on the position of the co-crystal ligand, where the binding pocket was formed by the amino acids His41, Met49, Phe140, Gly143, Ser144, Cys145, His163, His164, Glu166, Pro168, His172, Val186 and Gln189., The best docked conformation of enzyme-compound was analyzed based on the binding energy and active site interactions. Binding energy (kcal/mol) and enzyme(s) active site residues involved in interaction with the compounds are listed in Table 2. Binding energy values for the best conformation of chloroquine, hydroxychloroquine, remdesivir, HL and complex **1** with the spike protein / main protease are −4.40 / −6.47, −4.19 / −6.68, −3.78 / −7.16, −6.46 / −7.30 and −7.46 / −9.39 kcal/mol, respectively. HL and complex **1** showed higher binding energy than chloroquine, hydroxychloroquine and remdesivir, and interacted at the active site of the spike protein with Arg403, Glu406, Tyr453, Gln493, Tyr495, Phe497, Asn501, Tyr505, and Arg403, Tyr449, Tyr453, Gln493, Ser494, Tyr495, Phe497, Asn501, Tyr505 amino acids, respectively, and these interactions are well comparable with those of chloroquine, hydroxychloroquine and remdesivir.

HL and complex **1** displayed interactions with His41, Met49, Asn142, Ser144, Cys145, His163, Met165, Glu166, Asp187, Gln192, and Thr25, His41, Cys44, Tyr54, Met49, Cys145, His164, Asp187, Arg188, Gln192 active site residues of the main protease, respectively. Cys145–His41 catalytic dyad at the active site of the main protease is known to play an important role in the proteolytic activity. Both HL and complex **1** exhibited interactions with the catalytic dyad, indicating that these compounds may act as inhibitors of the main protease. Figs. 4 and 5 depict the best docked conformation of the compounds with SARS-

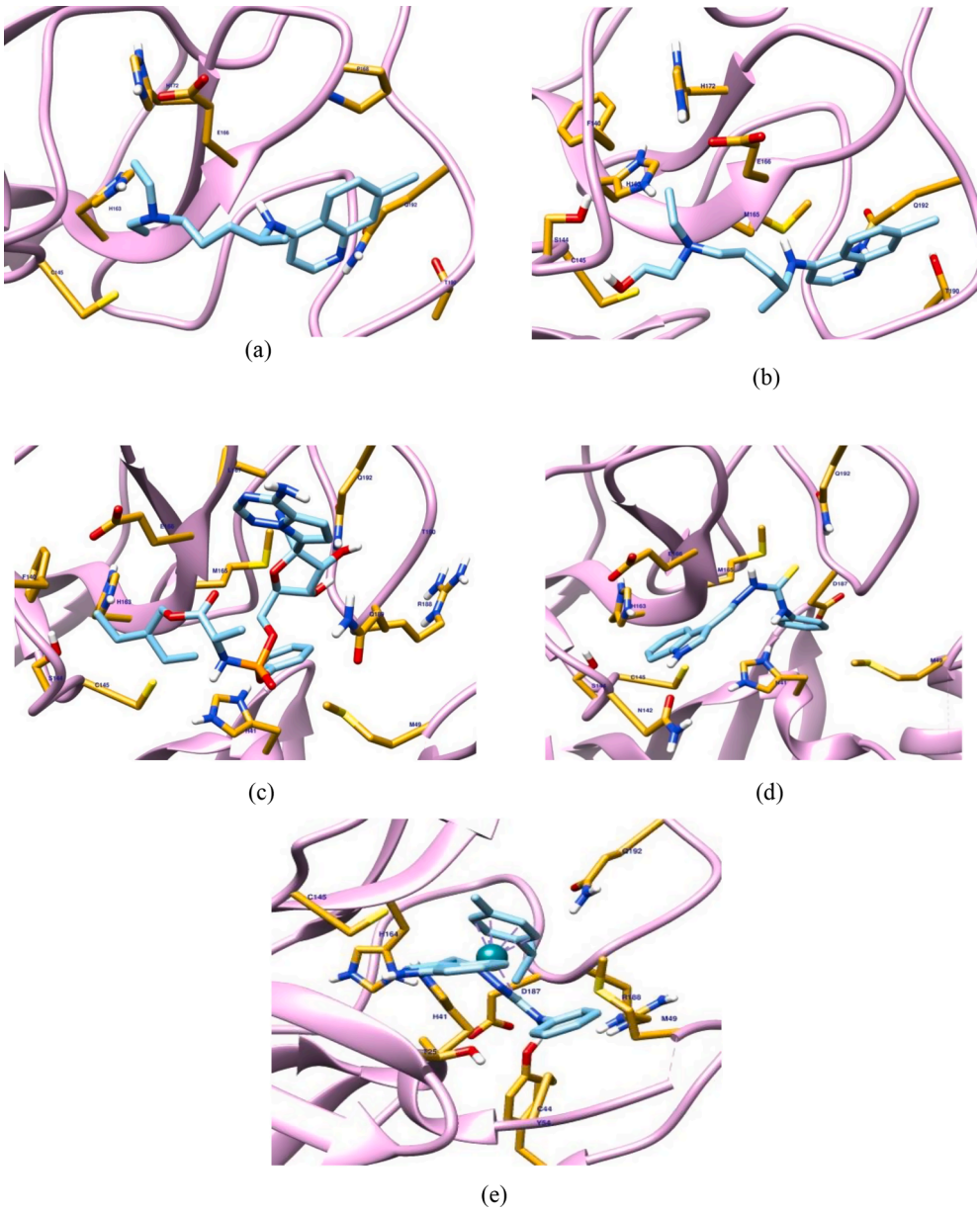

Fig. 5. Docked conformation of (a) chloroquine (b) hydroxychloroqine (c) remdesivir (d) HL and (e) complex **1** at the active site of SARS-CoV-2 main protease.

CoV-2 spike protein and main protease.

4. Conclusions

Water-soluble binuclear Ru(II)-*p*-cymene complex was prepared from indole thiosemicarbazone ligand in one step reaction and characterized by CHNS analysis, and various spectroscopic tools. The exact structure of complex was determined by X-ray diffraction study; the complex adopted a piano-stool geometry with two molecules of TSC coordinated to Ru(II) ion as bidentate monobasic ligand. The complex showed enhanced anticancer activity than the free ligand and cisplatin against A549, HeLa, HepG-2, T24 and EA.hy926 cancer cells. The complex displayed highest cytotoxicity against T24-bladder cancer cells. The cytotoxic potential of the complex was specific towards the cancer cells as in the normal cells such as Vero, lower cytotoxicity was observed. To screen the binding potential of compounds at the active sites of the spike protein and main protease of SARS-CoV-2, molecular docking studies were performed, and the results showed better binding energy. Active site interactions of HL and complex **1** are well comparable with chloroquine, hydroxychloroquine and remdesivir.

CRediT authorship contribution statement

Jebiti Haribabu: Writing – original draft, Investigation, Methodology. **Nithya Balakrishnan:** Writing – review & editing, Methodology. **Srividya Swaminathan:** Software, Formal analysis, Writing – review & editing. **Peter Jerome:** Software, Formal analysis, Writing – review & editing. **Dasararaju Gayathri:** Software, Formal analysis, Writing – review & editing. **Cesar Echeverria:** Software, Formal analysis, Writing – review & editing. **Nattamai Bhuvanesh:** Software, Formal analysis, Writing – review & editing, Supervision. **Ramasamy Karvembu:** Writing – original draft, Investigation, Methodology, Supervision.

Declaration of Competing Interest

The authors declare that they have no known competing financial interests or personal relationships that could have appeared to influence the work reported in this paper.

Acknowledgements

J. H. thanks the Fondo Nacional de Ciencia y Tecnologia (FONDECYT, 3200391 and 11170840). N. B. acknowledges the MHRD for financial assistance. S. S. thanks the Department of Science and Technology, Ministry of Science and Technology, Government of India, for doctoral fellowship under the DST-INSPIRE (IF160449) programme.

Appendix A. Supplementary material

All the spectra are depicted. Crystallographic data for the structures reported in this paper have been deposited with the Cambridge Crystallographic Data Centre (CCDC) as supplementary publication number (CCDC 2046159 for **1**). Copies of the data can be obtained free of charge from the CCDC (12 Union Road, Cambridge CB2 1EZ, UK; Tel.: + 44-1223-336408; Fax: + 44-1223-336003; e-mail: deposit@ccdc.cam.ac.uk; web site: http://www.ccdc.cam.ac.uk). Supplementary data to this article can be found online at https://doi.org/10.1016/j.inoche.2021.109029.

References

[1] Cancer Fact Sheet No. C53; World Health Organization, Globocan 2018, Retrieved March 2019.
[2] Y.-S. Sun, Z. Zhao, Z.-N. Yang, F. Xu, H.-J. Lu, Z.-Y. Zhu, W. Shi, J. Jiang, P.-P. Yao, H.-P. Zhu, Risk factors and preventions of breast cancer, Int. J. Biol. Sci. 13 (11) (2017) 1387–1397.
[3] R. Baskar, K.A. Lee, R. Yeo, K.W. Yeoh, Cancer and radiation therapy: Current advances and future directions, Int. J. Med. Sci. 9 (2012) 193–199.
[4] J. Haribabu, S. Srividya, D. Mahendiran, D. Gayathri, V. Venkatramu, N. Bhuvanesh, R. Karvembu, Synthesis of palladium(II) complexes *via* Michael addition: Antiproliferative effects through ROS-mediated mitochondrial apoptosis and docking with SARS-CoV-2, Inorg. Chem. 59 (2020) 17109–17122.
[5] T.C. Johnstone, G.Y. Park, S.J. Lippard, Understanding and improving platinum anticancer drugs - Phenanthriplatin, Anticancer Res. 34 (2014) 471–476.
[6] J.P.C. Coverdale, T. Laroiya-McCarron, I. Romero-Canelón, Designing ruthenium anticancer drugs: What have we learnt from the key drug candidates? Inorganics 7 (2019) 1–15.
[7] E. Alessio, L. Messori, Anticancer drug candidates face-to-face: A case story in medicinal inorganic chemistry, Molecules 24 (2019) 1–20.
[8] R. Trondl, P. Heffeter, C.R. Kowol, M.A. Jakupec, W. Berger, B.K. Keppler, NKP-1339, the first ruthenium-based anticancer drug on the edge to clinical application, Chem. Sci. 5 (8) (2014) 2925–2932.
[9] L.D. Dale, J.H. Tocher, T.M. Dyson, D.I. Edwards, D.A. Tocher, Studies on DNA damage and induction of SOS repair by novel multifunctional bioreducible compounds. II. A metronidazole adduct of a ruthenium-arene compound, Anti-Cancer Drug Des. 7 (1992) 3–14.
[10] C.G. Hartinger, N. Metzler-Nolte, P.J. Dyson, Challenges and opportunities in the development of organometallic anticancer drugs, Organometallics 31 (16) (2012) 5677–5685.
[11] R.E. Morris, R.E. Aird, P. del Socorro Murdoch, H. Chen, J. Cummings, N. D. Hughes, S. Parsons, A. Parkin, G. Boyd, D.I. Jodrell, P.J. Sadler, Inhibition of cancer cell growth by ruthenium(II)-arene complexes, J. Med. Chem. 44 (22) (2001) 3616–3621.
[12] W. Su, Q. Qian, P. Li, X. Lei, Q.i. Xiao, S. Huang, C. Huang, J. Cui, Synthesis, characterization and anticancer activity of a series of ketone-N^4-substituted thiosemicarbazones and their ruthenium(II)-arene complexes, Inorg. Chem. 52 (21) (2013) 12440–12449.
[13] M.K.M. Subarkhan, R. Ramesh, Ruthenium(II)-arene complexes containing benzhydrazone ligands: Synthesis, structure and antiproliferative activity, Inorg. Chem. Front. 3 (2016) 1245–1255.
[14] W. Guo, W. Zheng, Q. Luo, X. Li, Y. Zhao, S. Xiong, F. Wang, Transferrin serves as a mediator to deliver organometallic ruthenium(II) anticancer complexes into cells, Inorg. Chem. 52 (9) (2013) 5328–5338.
[15] J. Haribabu, S. Srividya, R. Umapathi, D. Gayathri, P. Venkatesu, N. Bhuvanesh, R. Karvembu, Enhanced anticancer activity of half-sandwich Ru(II)-*p*-cymene complex bearing heterocyclic hydrazone ligand, Inorg. Chem. Commun. 119 (2020) 108054–108062.
[16] V. Sharma, P. Kumar, D. Patha, Biological importance of the indole nucleus in recent years: A comprehensive review, J. Heterocycl. Chem. 47 (2010) 491–502.
[17] N. Balakrishnan, J. Haribabu, D. Anantha Krishnan, S. Swaminathan, D. Mahendiran, N.S.P. Bhuvanesh, R. Karvembu, Zinc(II) complexes of indole thiosemicarbazones: DNA/protein binding, molecular docking and *in vitro* cytotoxicity studies, Polyhedron 170 (2019) 188–201.
[18] J. Haribabu, M.M. Tamizh, C. Balachandran, Y. Arun, N.S.P. Bhuvanesh, Synthesis, structures and mechanistic pathways of anticancer activity of palladium(II) complexes with indole-3-carbaldehyde thiosemicarbazones, New J. Chem. 42 (2018) 10818–10832.
[19] J. Haribabu, K. Jeyalakshmi, Y. Arun, N.S.P. Bhuvanesh, P.T. Perumal, R. Karvembu, Synthesis, DNA/protein binding, molecular docking, DNA cleavage and *in vitro* anticancer activity of nickel(II) bis(thiosemicarbazone) complexes, RSC Adv. 5 (2015) 46031–46049.
[20] N. Balakrishnan, J. Haribabu, A.K. Dhanabalan, S. Swaminathan, S. Sun, D. F. Dibwe, N. Bhuvanesh, S. Awale, R. Karvembu, Thiosemicarbazone(s)-anchored water soluble mono- and bimetallic Cu(II) complexes: Enzyme-like activities, biomolecular interactions, anticancer property and real-time live cytotoxicity, Dalton Trans. 49 (2020) 9411–9424.
[21] F.A. Beckford, G. Leblanc, J. Thessing, M. Shaloski, B.J. Frost, L. Li, N.P. Seeram, Organometallic ruthenium complexes with thiosemicarbazone ligands: Synthesis, structure and cytotoxicity of $[(\eta^6\text{-}p\text{-cymene})Ru(NS)Cl]^+$ (NS = 9-anthraldehyde thiosemicarbazones), Inorg. Chem. Commun. 12 (2009) 1094–1098.
[22] J. Haribabu, G. Sabapathi, M.M. Tamizh, C. Balachandran, N.S.P. Bhuvanesh, P. Venuvanalingam, R. Karvembu, Water-soluble mono- and binuclear $Ru(\eta^6\text{-}p\text{-}$cymene) complexes containing indole thiosemicarbazones: Synthesis, DFT modeling, biomolcular interactions, and *in vitro* anticancer activity through apoptosis, Organometallics 37 (2018) 1242–1257.
[23] V.O. Yadhukrishnan, M. Muralisankar, R. Dheepika, R. Konakanchi, N.S. P. Bhuvanesh, S. Nagarajan, Structurally different domains embedded half-sandwich arene Ru(II) complex: DNA/HSA binding and cytotoxic studies, J. Coord. Chem. 73 (10) (2020) 1591–1604.
[24] W. Su, Z. Tang, P. Li, G. Wang, Q. Xiao, Y. Li, S. Huang, Y. Gu, Z. Lai, Y. Zhang, New dinuclear ruthenium-arene complexes containing thiosemicarbazone ligands: Synthesis, structure and cytotoxic studies, Dalton Trans. 45 (2016) 19329–19340.
[25] S. Swaminathan, J. Haribabu, N.K. Kalagatur, R. Konakanchi, N. Balakrishnan, N. Bhuvanesh, R. Karvembu, Synthesis and anticancer activity of $[RuCl_2(\eta^6\text{-arene})$ (aroylthiourea)] complexes - High activity against the human neuroblastoma (IMR-32) cancer cell line, ACS Omega 4 (4) (2019) 6245–6256.
[26] K. Jeyalakshmi, J. Haribabu, C. Balachandran, S. Swaminathan, N.S.P. Bhuvanesh, R. Karvembu, Coordination behavior of N, N′, N″-trisubstituted guanidine ligands in their Ru-arene complexes: Synthetic, DNA/protein binding, and cytotoxic studies, Organometallics 38 (2019) 753–770.
[27] K. Jeyalakshmi, J. Haribabu, C. Balachandran, E. Narmatha, N.S.P. Bhuvanesh, S. Aoki, S. Awale, R. Karvembu, Highly active copper(I) complexes of aroylthiourea ligands against cancer cells - Synthetic and biological studies, New J. Chem. 43 (2019) 3188–3198.
[28] K. Jeyalakshmi, J. Haribabu, N.S.P. Bhuvanesh, R. Karvembu, Half-sandwich $RuCl_2(\eta^6\text{-}p\text{-cymene})$ core complexes containing sulfur donor aroylthiourea ligands: DNA and protein binding, DNA cleavage and cytotoxic studies, Dalton Trans. 45 (2016) 12518–12531.
[29] F. Li, J.G. Collins, F.R. Keene, Ruthenium complexes as antimicrobial agents, Chem. Soc. Rev. 44 (8) (2015) 2529–2542.
[30] J. Haribabu, D.S. Ranade, N.S.P. Bhuvanesh, P.P. Kulkarni, R. Karvembu, Ru(II)-*p*-cymene thiosemicarbazone complexes as inhibitors of amyloid β (Aβ) peptide aggregation and Aβ-induced cytotoxicity, ChemistrySelect 2 (35) (2017) 11638–11644.
[31] G.M. Sheldrick, A short history of SHELX, Acta Crystallogr. Sect. A Found. Crystallogr. 64 (1) (2008) 112–122.
[32] G.M. Sheldrick, Crystal structure refinement with SHELXL, Acta Crystallogr, Sect. C. Struct. Chem. 71 (1) (2015) 3–8.
[33] G.M. Sheldrick, SHELXT - Integrated space-group and crystal-structure determination, Acta Crystallogr. Sect. A Found. Crystallogr. 71 (1) (2015) 3–8.
[34] A.L. Spek, Single-crystal structure validation with the program PLATON, J. Appl. Crystallogr. 36 (1) (2003) 7–13.
[35] O.V. Dolomanov, L.J. Bourhis, R.J. Gildea, J.A.K. Howard, H. Puschmann, OLEX2: A complete structure solution, refinement and analysis program, J. Appl. Crystallogr. 42 (2009) 339–341.
[36] P. Bindu, M.R.P. Kurup, T.R. Satyakeerty, EPR, cyclic voltammetric and biological activities of copper(II) complexes of salicylaldehyde N(4)-substituted thiosemicarbazone and heterocyclic bases, Polyhedron 18 (3-4) (1998) 321–331.
[37] E.F. Pettersen, T.D. Goddard, C.C. Huang, G.S. Couch, D.M. Greenblatt, E.C. Meng, T.E. Ferrin, UCSF Chimera - A visualization system for exploratory research and analysis, J. Comput. Chem. 25 (13) (2004) 1605–1612.
[38] G.M. Morris, R. Huey, A.J. Olson, Using AutoDock for ligand-receptor docking, Curr. Protoc. Bioinformatics 24 (2008) 8–14.
[39] H.M. Berman, J. Westbrook, Z. Feng, G. Gilliland, T.N. Bhat, H. Weissig, I. N. Shindyalov, P.E. Bourne, The protein data bank, Nucleic Acids Res. 28 (2000) 235–242.
[40] S.K. Burley, H.M. Berman, C. Bhikadiya, C. Bi, L. Chen, L. Di Costanzo, C. Christie, K. Dalenberg, J.M. Duarte, S. Dutta, Z. Feng, S. Ghosh, D.S. Goodsell, D. Guzenko, B.P. Hudson, T. Kalro, K. Green, V. Guranovi, Y. Liang, R. Lowe, H. Namkoong, E. Peisach, I. Periskova, A. Prlic, C. Randle, A. Rose, P. Rose, R. Sala, M. Sekharan, C. Shao, L. Tan, Y.P. Tao, Y. Valasatava, M. Voigt, J. Westbrook, J. Woo, H. Yang, J. Young, M. Zhuravleva, C. Zardecki, RCSB protein data bank: Biological macromolecular structures enabling research and education in fundamental biology, biomedicine, biotechnology and energy, Nucleic Acids Res. 47 (2019) 464–474.
[41] J. Lan, J. Ge, J. Yu, S. Shan, H. Zhou, S. Fan, Q.i. Zhang, X. Shi, Q. Wang, L. Zhang, X. Wang, Structure of the SARS-CoV-2 spike receptor-binding domain bound to the ACE2 receptor, Nature 581 (7807) (2020) 215–220.
[42] L. Zhang, D. Lin, X. Sun, U. Curth, C. Drosten, L. Sauerhering, S. Becker, K. Rox, R. Hilgenfeld, Crystal structure of SARS-CoV-2 main protease provides a basis for design of improved α-ketoamide inhibitors, Science 368 (2020) 409–412.
[43] B. Demoro, C. Sarniguet, R.S. Delgado, M. Rossi, D. Liebowitz, F. Caruso, C. Olea-Azar, V. Moreno, A. Medeiros, M.A. Comini, L. Otero, D. Gambino, New

organoruthenium complexes with bioactive thiosemicarbazones as co-ligands: Potential anti-trypanosomal agents, Dalton Trans. 41 (2012) 1534–1543.
[44] J. Haribabu, C. Balachandran, M.M. Tamizh, Y. Arun, N.S.P. Bhuvanesh, S. Aoki, R. Karvembu, Unprecedented formation of palladium(II)-pyrazole based thiourea from chromone thiosemicarbazone and $[PdCl_2(PPh_3)_2]$: Interaction with biomolecules and apoptosis through mitochondrial signaling pathway, J. Inorg. Biochem. 205 (2020) 110988–110999.
[45] P.J. Jarman, F. Noakes, S. Fairbanks, K. Smitten, I.K. Griffiths, H.K. Saeed, J. A. Thomas, C. Smythe, Exploring the cytotoxicity, uptake, cellular response and proteomics of mono- and dinuclear DNA light-switch complexes, J. Am. Chem. Soc. 141 (2019) 2925–2937.
[46] A.I.T. Bruno Demoro, R.F.M. de Almeida, F. Marques, C.P. Matos, L. Otero, J. C. Pessoa, I. Santos, A. Rodríguez, V. Moreno, J. Lorenzo, D. Gambino, Screening organometallic binuclear thiosemicarbazone ruthenium complexes as potential anti-tumour agents: Cytotoxic activity and human serum albumin binding mechanism, Dalton Trans. 42 (2013) 7131–7146.
[47] Y. Zhong, X. Li, J. Chen, X. Wang, L. Wei, L. Fang, A. Kumar, S. Zhuang, J. Liu, Recent advances in MOF-based nanoplatforms generating reactive species for chemodynamic therapy, Dalton Trans. 49 (32) (2020) 11045–11058.
[48] W. Liu, Q. Yan, C. Xia, X. Wang, A. Kumar, Y. Wang, Y. Liu, Y. Pan, J. Liu, Recent advances in cell membrane coated metal–organic frameworks (MOFs) for tumor therapy, J. Mater. Chem. B. 9 (22) (2021) 4459–4474.
[49] J.-J. Xue, F. Bigdeli, J.-P. Liu, M.-L. Hu, A. Morsali, Ultrasonic-assisted synthesis and DNA interaction studies of two new Ru complexes; RuO_2 nanoparticles preparation, Nanomedicine (Lond.) 13 (21) (2018) 2691–2708.
[50] W. Liu, Y. Pan, Y. Zhong, B. Li, Q. Ding, H. Xu, Y. Qiu, F. Ren, B. Li, M. Muddassir, J. Liu, A multifunctional aminated UiO-67 metal-organic framework for enhancing antitumor cytotoxicity through bimodal drug delivery, Chem. Eng. J. 412 (2021), 127899.
[51] S. Swaminathan, J. Haribabu, M.K.M. Subarkhan, D. Gayathri, N. Balakrishnan, N. Bhuvanesh, C. Echeverria, R. Karvembu, Impact of aliphatic acyl and aromatic thioamide substituents on the anticancer activity of Ru(II)-*p*-cymene complexes with acylthiourea ligands – *In vitro* and *in vivo* studies, Dalton Trans (2021), https://doi.org/10.1039/d1dt02611a.
[52] S.A. Kulkarni, S.K. Nagarajan, V. Ramesh, V. Palaniyandi, S.P. Selvam, T. Madhavan, Computational evaluation of major components from plant essential oils as potent inhibitors, J. Mol. Struct. 1221 (2020), 128823.